

# Excellence in Chemistry Research

## Announcing our new flagship journal

- Gold Open Access
- Publishing charges waived
- Preprints welcome
- Edited by active scientists



## Meet the Editors of *ChemistryEurope*



**Luisa De Cola**

Università degli Studi  
di Milano Statale, Italy



**Ive Hermans**

University of  
Wisconsin-Madison, USA



**Ken Tanaka**

Tokyo Institute of  
Technology, Japan

# Chitosan-Silica as a Cheap Carrier and Green Soft Ligand for Improved Ru-catalyzed Hydroformylation

Francisco Javier Escobar-Bedia,<sup>[a]</sup> Vlad Martin-Diaconescu,<sup>[b]</sup> Laura Simonelli,<sup>[b]</sup> Maria J. Sabater,<sup>\*[a]</sup> and Patricia Concepción<sup>\*[a]</sup>

Dodecacarbonyltriruthenium  $\text{Ru}_3(\text{CO})_{12}$  has been immobilized onto a biopolymer (chitosan) supported on  $\text{SiO}_2$  ( $\text{Ch@SiO}_2$ ) to give  $\text{Ru-Ch@SiO}_2$ .  $\text{Ch@SiO}_2$  behaves as a soft, recoverable and bulky ligand allowing the stabilization of released Ru active species and preventing its irreversible reduction to  $\text{Ru}^0$ . Under these conditions very high activity ( $\text{TOF} = 1086 \text{ h}^{-1}$ ;  $\text{TON} = 2749$ ) and regioselectivity ( $n:\text{iso} = 92:8$ ) are obtained, surpassing that of the homogeneous  $\text{Ru}_3(\text{CO})_{12}$  counterpart.

Spectroscopic studies have shown that  $\text{Ru}_3(\text{CO})_{12}$  transforms into a mononuclear  $\text{Ru}^{n+}$  ( $n = 2,3$ ) di- or tri-carbonyl species by interacting with the amido/amino groups of the biopolymer,

being released into the reaction media whilst stabilized by the chitosan functional groups.

The herein  $0.5 \text{ Ru-Ch@SiO}_2$  catalyst can operate be operated under a semi-continuous mode for at least 14 h without deactivation, representing providing a starting point in the search for a green catalyst with definitive industrial application in hydroformylations. In particular in the search for a heterogeneous catalyst away from the use of phosphines and their known drawbacks (i.e. tedious synthesis, facile oxidation of phosphor center, ..) as well as expensive Rh as active site.

## Introduction

Since Roelen's discovery in 1938,<sup>[1]</sup> the hydroformylation reaction has become a highly relevant reaction at industrial level, reaching an annual production of over 10 million metric tons of aliphatic aldehydes and revealing itself as the greater example of homogeneous catalysis at industrial scale.<sup>[2]</sup> Aldehydes are a high value specialty product but also a bulk chemical commodity, due to the reactivity of the CHO moiety that allows easy access to different compounds such as alcohols, carboxylic acids, amines, and imines, thus becoming the raw material for many important products (i.e. fine chemicals, drugs, flavors, fragrances, polymers, etc).<sup>[3,4]</sup>

In order to meet the growing demand of the highly desired aldehydes great efforts have been invested in the development of improved catalytic systems in which ligands play a pivotal role. Indeed, the early unmodified  $\text{Co}_2(\text{CO})_8$  catalyst quickly became obsolete when Mullineaux and Pruett showed the great

promoting effect that phosphine ligands had on the selectivity and regioselectivity of the reaction for obtaining aldehydes from alkenes.<sup>[5,6]</sup> The importance of these outcomes led to the development of the Shell Higher Olefin process,<sup>[7]</sup> which is still operational today for the production of fatty alcohols by hydrogenation of the respective aldehyde.<sup>[8]</sup> Later, Wilkinson applied the newly discovered promoting and stabilizing effect of the  $\text{PPh}_3$  ligand to rhodium,<sup>[9]</sup> a much more expensive but also reactive metal, leading to the Low Pressure Oxo process (LPO). The great success of the LPO process caused the phosphine-based ligands to become the backbone of all modern hydroformylation processes and major efforts were made to further improve their viability performance as catalysts.

In this direction, the development of new ligands such as water soluble phosphines,<sup>[10-18]</sup> phosphonites or more recently nitrogen based compounds have appeared in the literature.<sup>[19-23]</sup> although most of them require of complex synthesis procedures to aid in catalyst recovery and facilitate the scaling process, hence limiting their industrial application. In parallel, together with the search for new organic ligands, other metals, such as ruthenium, iridium, iron, platinum, or palladium, have been also investigated to tune the intrinsic catalytic properties of the metal.<sup>[24-33]</sup> Regarding ruthenium based catalysts, it has been reported that in general mononuclear carbonyl ruthenium complexes exhibit higher activity and selectivity than polynuclear complexes so that their activity and selectivity can be tuned by a suitable ligand system.<sup>[34-37]</sup> This is the case of  $\text{Ru}_3(\text{CO})_{12}$  which when combined with an imidazolyl-substituted monophosphine and other heterocycle-derived phosphine ligands can provide good activities and tunable selectivity towards the aldehyde and/or alcohol.<sup>[38-40]</sup> In this case,  $\text{Ru}_3(\text{CO})_{12}$  has been considered as a pre-catalyst of a new active species, identified as  $\text{HRu}(\text{CO})_3\text{L}$ , which is formed under reaction conditions.<sup>[39]</sup> However the nature and oxidation state of the

[a] Dr. F. J. Escobar-Bedia, Dr. M. J. Sabater, Dr. P. Concepción  
 Instituto de Tecnología Química  
 Universitat Politècnica de València-Consejo Superior  
 de Investigaciones Científicas (UPV-CSIC)  
 Avenida de los Naranjos s/n  
 46022 Valencia (Spain)  
 E-mail: mjsabate@itq.upv.es  
 pconcepc@upvnet.upv.es

[b] Dr. V. Martin-Diaconescu, Dr. L. Simonelli  
 CELLS – ALBA Synchrotron Radiation Facility  
 Carrer de la Llum 2–26  
 08290 Cerdanyola del Vallès (Spain)

Supporting information for this article is available on the WWW under <https://doi.org/10.1002/cctc.202200861>

© 2022 The Authors. ChemCatChem published by Wiley-VCH GmbH. This is an open access article under the terms of the Creative Commons Attribution License, which permits use, distribution and reproduction in any medium, provided the original work is properly cited.

mononuclear ruthenium active site has not been reported disclosed so far. In addition, other Ru precursors, such as homogeneous and heterogeneous Ru(II) and Ru(III) complexes have been also explored.<sup>[41–43]</sup>

Despite all these advances, short and easily scalable syntheses methods that are economically viable, green, and safe to the point of avoiding the use of flammable and/or toxic phosphines are necessary for large scale hydroformylation plants.<sup>[44]</sup> To this respect, intensive efforts have been focused on the immobilization of homogeneous catalysts on inorganic/organic compounds (i.e. polymers, zeolites, polyoxometalates, ...), which in some cases mimic the behavior of soft ligands and modulate the leaching of active sites through a dynamic anchoring/release process avoiding their irreversible reduction toward metallic agglomerates.<sup>[45]</sup>

Thus, with these goals ahead, we have devised an easily available, cheap hybrid organic-inorganic mild ligand for  $\text{Ru}_3(\text{CO})_{12}$  that consists of an organic layer composed of chitosan supported on an inorganic layer of  $\text{SiO}_2$  ( $\text{Ch@SiO}_2$ ). This composite will behave simultaneously as a recoverable carrier and as a soft ligand of the homogeneous  $\text{Ru}_3(\text{CO})_{12}$  catalyst.

Chitosan is a natural containing biopolymer with low surface area ( $<3 \text{ m}^2/\text{g}$ ) obtained from deacetylation of chitin, whose polymeric chain is composed by  $\beta$  (1-4) D-glucosamine and N-acetyl-D glucosamine units (Figure 1).<sup>[46–49]</sup>

The physicochemical characteristics and functional properties of chitosan (i.e. polycationic character, biocompatibility, ..) make this polysaccharide of interest in different fields.<sup>[46–49]</sup> In this context, a way to increase its surface area and improve the accessibility of functional groups consists of supporting chitosan on a solid with higher surface area (i.e.  $\text{SiO}_2$ ) to give a composite with improved textural parameters named  $\text{Ch@SiO}_2$  (see characterization data in SI).<sup>[49]</sup> Thus, in this work we will show that the combination of  $\text{Ru}_3(\text{CO})_{12}$  and the hybrid  $\text{Ch@SiO}_2$  acting as a weak and recoverable ligand, will give rise to a highly active and regioselective catalyst for the hydroformylation of 1-hexene, without the need of using phosphines or similar ligands. Indeed  $\text{Ru}_3(\text{CO})_{12}$  transforms into a new catalytic

active complex, which is stabilized under reaction conditions by means of weak interactions with the functional groups of the chitosan@silica composite, preventing in this way its irreversible reduction to the inactive  $\text{Ru}^0$ .

## Results and Discussion

### Synthesis and characterization

$0.5\text{Ru}-\text{Ch@SiO}_2$  was prepared following an impregnation method by using a solution of  $\text{Ru}_3(\text{CO})_{12}$  in n-pentane and the hybrid material  $\text{Ch@SiO}_2$ ,<sup>[46,49]</sup> followed by complete evaporation of the solvent (details in the experimental section). Inductive coupled plasma optical emission spectrometry (ICP) and elemental analysis revealed a 0.5 wt% incorporation Ru in the  $\text{Ru}-\text{Ch@SiO}_2$  catalyst as well as 1.5 wt% N and 8.1 wt% C, associated to the chitosan component. The C/N ratio, a parameter directly related to the degree of deacetylation (DDA) of chitosan remained unchanged after incorporating Ru ( $\text{C/N} = 5.4$ ), indicating that no major structure changes occurred during the preparation of the catalyst. In this respect,  $^{13}\text{C}$  CP MAS-NMR (Fig.S2, and details in SI), confirmed that the structure of the chitosan monomer was preserved after  $\text{Ru}_3(\text{CO})_{12}$  incorporation. More details in the physical-chemical catalyst characterization can be found in the SI.

### Catalytic performance

The catalytic system comprised of  $\text{Ru}_3(\text{CO})_{12}$  impregnated on chitosan-silica ( $0.5\text{Ru}-\text{Ch@SiO}_2$ ) was tested in the hydroformylation reaction using 1-hexene as a model substrate (scheme 1). The 1-hexene conversion and the selectivity to the main products is given in table 1, entry 7. Under the conditions indicated in table 1 (40 bar  $\text{CO}:\text{H}_2$  (1:1),  $170^\circ\text{C}$ , 0.022% mmol Ru and 2 ml NMP) 88% conversion, 66% aldehyde selectivity and a linear/branched aldehyde ratio of 92:8 was obtained

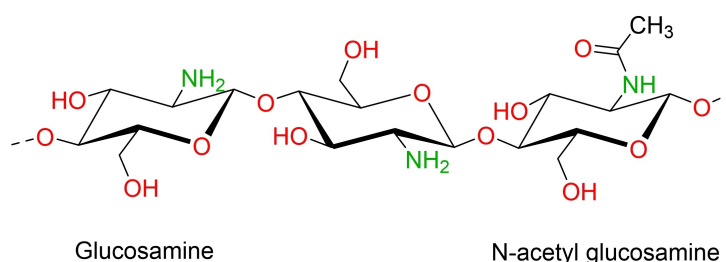
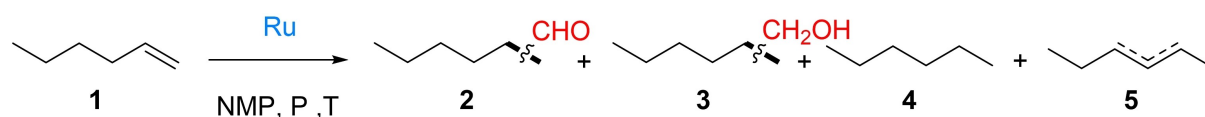
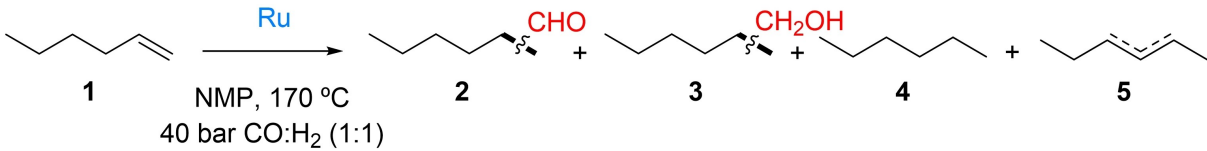


**Figure 1.** Chitosan structure of a partially deacetylated chitosan showing both amino (glucosamine) and amide (N-acetyl glucosamine) units.



**Scheme 1.** Hydroformylation of 1-hexene with a ruthenium catalytic system.

**Table 1.** Catalytic activity of Ru<sub>3</sub>(CO)<sub>12</sub> based systems for the hydroformylation of 1-hexene.<sup>[a]</sup>



Entry	Catalytic System	Conv. <sup>[a]</sup> [%]	Yield [%] 2 (n:iso) <sup>[b]</sup>	3 (n:iso)	4	5	TON [ <sup>c</sup> ]	TOF [ <sup>d</sup> ] [h <sup>-1</sup> ]
1	Ru <sub>3</sub> (CO) <sub>12</sub>	83	22 (83:17)	0 (-)	8	53	1197	180
2	Ru <sub>3</sub> (CO) <sub>12</sub> + PPh <sub>3</sub>	92	28 (78:22)	0 (-)	8	56	1214	205
3	Ru <sub>3</sub> (CO) <sub>12</sub> + Xantphos	74	24 (89:11)	0 (-)	5	45	1085	221
4	Ru <sub>3</sub> (CO) <sub>12</sub> + Chitosan	83	26 (82:18)	0 (-)	7	50	1329	180
5	Ru <sub>3</sub> (CO) <sub>12</sub> + SiO <sub>2</sub>	85	18 (80:20)	0 (-)	10	57	965	220
6	Ru <sub>3</sub> (CO) <sub>12</sub> + Ch@SiO <sub>2</sub>	84	24 (84:16)	0 (-)	8	52	1227	217
7	0.5Ru–Ch@SiO <sub>2</sub> <sup>[e]</sup>	92	61 (92:8)	4 (100:0)	3	24	2755	1087
8	0.5Ru–Ch@SiO <sub>2</sub> <sup>[f]</sup>	82	9 (74:26)	0 (-)	24	49	436	43

after 7 h of reaction. Moreover, turnover frequency (TOF) and turnover number (TON) values of 1087 h<sup>-1</sup> and 2755 were obtained respectively, greatly exceeding the values obtained with the corresponding homogeneous catalyst Ru<sub>3</sub>(CO)<sub>12</sub> (table 1, entry 1).

Thus, in order to define the nature of active species, hot filtration experiments have been carried out using the 0.5Ru–Ch@SiO<sub>2</sub> catalyst and the catalytic results obtained from both the liquid and the solid after filtration are displayed in Figure 2.

As can be seen from Figure 2.A, the hot filtration test was performed after 0.5 h of reaction, during the most active phase of the catalyst and both the filtered solid (○) and the recovered liquid (●) were subjected to a second reaction run under the same conditions. Thus, after filtration, the solid (Figure 2.A, ○) showed a complete loss of catalytic activity that could be attributed to the migration of Ru species to the reaction media given that the supported solid contained 0.01 % wt. Ru after the first use as determined by ICP-AES. From this result, it could also be deduced that Ch@SiO<sub>2</sub> (○) showed no intrinsic catalytic activity towards hydroformylation or isomerization in the absence of ruthenium metal. In the case of the recovered liquid (Figure 2.A, ●), it showed a catalytic behavior that closely resembled that of the original Ru<sub>3</sub>(CO)<sub>12</sub> cluster (Figure 2.A, ▼) characterized by a lower activity and regioselectivity than that of the original 0.5Ru–Ch@SiO<sub>2</sub> hybrid material (Figure 2.A, ■).

These results strongly point that the ruthenium species are released into the reaction medium from the 0.5Ru–Ch@SiO<sub>2</sub> catalyst under reaction conditions, but must be stabilized by

the Ch@SiO<sub>2</sub> composite, which in turn will modulate the nature of active sites in the way that will be described later.

Interestingly, when 0.5Ru–Ch@SiO<sub>2</sub> was present in the reaction mixture the hydrogenating capacity of Ru species was greatly reduced from 10% for Ru<sub>3</sub>(CO)<sub>12</sub> to 3% for the 0.5Ru–Ch@SiO<sub>2</sub> material, leaving the isomerization reaction of 1-hexene to 2-hexene as the only major side reaction (Figure 2B). In addition, in the presence of the 0.5Ru–Ch@SiO<sub>2</sub> catalyst the hydroformylation pathway was favored over the isomerization as noted by the important increase of aldehyde selectivity from ca. 27% for the homogeneous carbonyl cluster up to 66% for the 0.5Ru–Ch@SiO<sub>2</sub> material, which in turn led to a remarkable increase in the TON and TOF values (see table 1). Additionally, the composite catalyst showed a greater selectivity towards the anti-Markovnikov addition of the hydride allowing for much greater region-control, by obtaining up to 92% of the lineal aldehyde n-heptanal as the major product along with small amounts of 2-methylhexanal (Figure 2B).

From the data in Figure 2A and the loss of activity observed for the recovered 0.5Ru–Ch@SiO<sub>2</sub> catalyst, it is clear that neither the Ru species of the filtrate (●) nor the filtered solid composite (○) retain the activity observed in the starting 0.5Ru–Ch@SiO<sub>2</sub> (■) catalyst. However, a combination of both (Ru and Ch@SiO<sub>2</sub>) is necessary to get a competitive catalyst that outperforms the original homogeneous Ru catalyst (Ru<sub>3</sub>(CO)<sub>12</sub>).

So next, the long-term stability of the 0.5Ru–Ch@SiO<sub>2</sub> composite was tested in semi-continuous operating mode in which a second addition of fresh 1-hexene was performed after

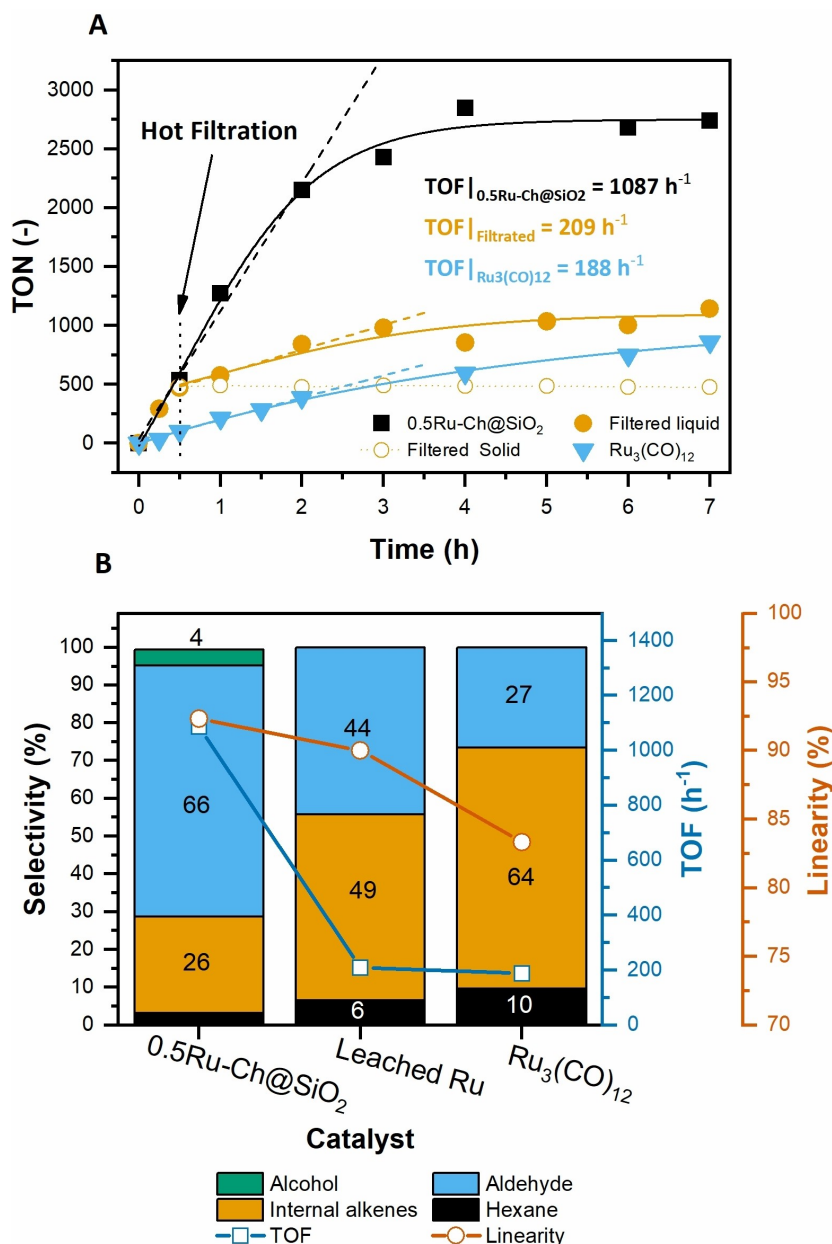


**Figure 2.** (A) Turnover number vs reaction time and (B) product distribution (columns), Turnover Frequency (TOF) (scatter-square) and linear to branched ratio (linearity, scatter-circles) for the different catalysts after 7 h of reaction.

one catalytic run, thus allowing to determine the lifetime of the Ru based catalyst (Figure 3).

From Figure 3 it can be deduced that the catalyst can perform a second reaction cycle with a slight reduction in catalytic activity while retaining the initial regioselectivity.

In summary, despite the fact that the reaction takes place in the liquid phase, the presence of the solid Ch@SiO<sub>2</sub> behaving as a soft ligand is crucial to obtain a competitive and stable catalyst with a higher half-life compared to the original commercial Ru<sub>3</sub>(CO)<sub>12</sub> catalyst. Definitely, it appears that the reaction is neither completely homogeneous nor completely heterogeneous, so that it could be taking place at the liquid/solid interface of the biphasic system.

Then an in-depth catalytic and spectroscopic study was performed in order to get insight into the ruthenium active species and the role of the Ch@SiO<sub>2</sub> composite. Therefore, in a first approximation and in order to determine whether a single component or the entire nanocomposite Ch@SiO<sub>2</sub> were responsible for the improved catalytic activity, different reactions were carried out by mixing the carbonyl cluster Ru<sub>3</sub>(CO)<sub>12</sub> with isolated chitosan (Ch), SiO<sub>2</sub> or Ch@SiO<sub>2</sub> directly inside the reactor vessel (skipping the impregnation procedure). Then, the obtained results (entries 4–6, Table 1) were compared with those of the 0.5Ru–Ch@SiO<sub>2</sub> nanocomposite (entry 7, Table 1).

As shown in table 1 only when the catalyst is prepared via the impregnation procedure (Entry 7, Table 1) an improvement

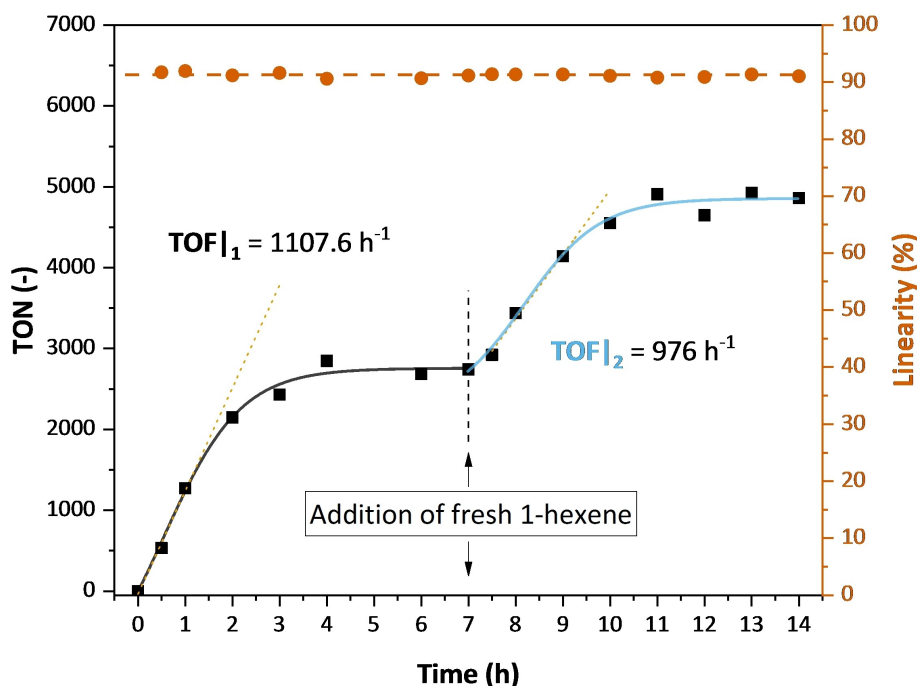


Figure 3. Kinetic data for the 0.5Ru–Ch@SiO<sub>2</sub> material before and after the addition of fresh 1-hexene in semi-continuous operation in a batch reactor.

in the catalytic performance is obtained. On the contrary, when Ch, SiO<sub>2</sub> or Ch@SiO<sub>2</sub> and Ru<sub>3</sub>(CO)<sub>12</sub> are added separately the catalytic behavior (entries 4, 5 and 6, Table 1) remains unaffected, so that it closely resembles that of the Ru<sub>3</sub>(CO)<sub>12</sub> catalyst without any additive (Entry 1, Table 1).

In addition, the activity of two catalytic systems comprised of Ru<sub>3</sub>(CO)<sub>12</sub> and two well-known typical phosphines such as PPh<sub>3</sub> and Xantphos commonly used in hydroformylations (entries 2 and 3, Table 1), were compared with that of 0.5Ru–Ch@SiO<sub>2</sub>.<sup>[50]</sup> We obtained that the influence of both phosphines on the catalytic performance of Ru<sub>3</sub>(CO)<sub>12</sub> was of the same order as with separately added Ch@SiO<sub>2</sub> (entry 6, Table 1) and markedly lower than that of the as-prepared 0.5Ru–Ch@SiO<sub>2</sub> catalyst (entry 7, Table 1).

### Spectroscopic insight into the nature of active species

Next, spectroscopic studies were done in order to get insight into the nature of active sites. In a first approach, Ru<sub>3</sub>(CO)<sub>12</sub> dissolved in NMP (used as solvent) was initially studied. In this regard, it is known the beneficial role of NMP in hydroformylation reactions, which has been usually ascribed to its basicity and high CO<sub>2</sub> solubility.<sup>[51–53]</sup> Interestingly, IR spectroscopy, supported by X-ray adsorption spectroscopy (XAS) (the last discussed in the next section), allowed to observe a disruption of the Ru<sub>3</sub>(CO)<sub>12</sub> complex in the presence of NMP, which was not observed when using other solvents like toluene.

Effectively, as shown in Figure S4, the IR spectra of Ru<sub>3</sub>(CO)<sub>12</sub> dissolved in NMP, (Figure S4b, red line) resulted in three IR

bands at 2055, 1982 and 1936 cm<sup>-1</sup>, differing from those reported in the literature for Ru<sub>3</sub>(CO)<sub>12</sub> (IR bands at 2075, 2049, 2016, 1997 and 1982 cm<sup>-1</sup>) or the Ru<sub>3</sub>(CO)<sub>12</sub> dissolved in toluene (Figure S4a).<sup>[54]</sup> The disappearance of the IR bands ascribed to Ru<sub>3</sub>(CO)<sub>12</sub> when interacting with NMP points to a non-innocent role of the solvent, which to our knowledge, has not been reported so far in hydroformylations.

More importantly, Ru<sub>3</sub>(CO)<sub>12</sub> catalyst dissolved in NMP shows similar infrared bands to those obtained with the fresh 0.5Ru–Ch@SiO<sub>2</sub> composite (Figure S4b, blue line), which strongly points to the formation of similar ruthenium carbonyl complexes in both cases, while different from the Ru<sub>3</sub>(CO)<sub>12</sub> starting precursor complex.

Decarbonylation of Ru<sub>3</sub>(CO)<sub>12</sub> by a ligand replacement reaction between the hydroxyl groups of the support and CO has already been described in the literature. In addition, it has been shown that the oxygen atoms of the support can react nucleophilically with the Ru atoms weakening and breaking the Ru–Ru bond of the Ru<sub>3</sub>(CO)<sub>12</sub> complex, resulting in monomeric ruthenium species.<sup>[55–57]</sup> In the same direction, according to Ali et al.,<sup>[58]</sup> the interaction between bidentate Schiff bases and Ru<sub>3</sub>(CO)<sub>12</sub> results in the formation of mononuclear [Ru<sup>2+</sup>(CO)<sub>3</sub>L] complexes, which display similar IR bands as in our case, i.e. at 2052, 1981 and 1941 cm<sup>-1</sup>. In addition, similar IR bands at 2060–2057 and 2000–1980 cm<sup>-1</sup> have been ascribed to mononuclear Ru<sup>n+</sup> (n=2,3) di or tricarbonyl complexes by other authors in the literature,<sup>[59–60]</sup> while polynuclear ruthenium carbonyl complexes are characterized by an IR band around 1975 cm<sup>-1</sup>, associated to bridge CO.<sup>[55]</sup>

Based on this data and considering the IR spectra displayed in Figure S4b, we speculated on the formation of mononuclear

$\text{Ru}^{n+}$  ( $n=2,3$ ) carbonyl complexes by a partial disruption of the  $\text{Ru}_3(\text{CO})_{12}$  cluster, induced by functional groups of the NMP and/or chitosan biopolymer. In fact, the IR spectra of the  $\text{Ch@SiO}_2$  composite, which displayed a sharp band at 1662 and  $3391\text{ cm}^{-1}$  due to the carbonyl group of the amido functionality and amino groups respectively, shifted after  $\text{Ru}_3(\text{CO})_{12}$  loading, indicating interaction through those functional groups (Figure S5). If this is so, a similar interaction through the carbonyl group of NMP could be expected.

Definitely we could confirm that  $\text{Ru}_3(\text{CO})_{12}$  behaves as a precatalyst, as already suggested by Beller et al.,<sup>[39]</sup> surely by transforming into a mononuclear  $\text{Ru}^{n+}(\text{CO})_x\text{L}$  species ( $n$  and  $x=2,3$ ) by the action of ligands. In this respect, the point that the reactive species is mononuclear Ru rather than the  $\text{Ru}_3(\text{CO})_{12}$  carbonyl complex is supported by the fact that when using toluene as solvent, the  $\text{Ru}_3(\text{CO})_{12}$  cluster is preserved from being transformed, and its activity for hydroformylation is very low (table 1, entry 8).

Thus, although the IR data point to the fact that the formation of mononuclear ruthenium species induced by the presence of NMP and those formed on the solid composite  $\text{Ch@SiO}_2$  after loading  $\text{Ru}_3(\text{CO})_{12}$  are very similar in nature (Figure S4b), the question remains open as to why both catalysts show different catalytic behavior, as displayed in Figure 2 and compiled into table 1 (entries 1 and 7). A priori, this fact should be related to a different nature and/or evolution of active species under reaction conditions.

Effectively, as ensured from the hot filtration experiments, ruthenium species in the  $0.5\text{Ru}-\text{Ch@SiO}_2$  sample are released to the liquid phase under reaction conditions (Figure 2A). However, the nature and stability of these ruthenium species in solution may be different (as will be discussed below based on XAS analysis) and strongly dependent on the environment around the metal center under operating conditions. That is, in the presence of only NMP (filtered liquid) a fast reduction to  $\text{Ru}^0$  takes place, whereas a concomitant loss of catalytic activity is observed (Figure 2A). This is confirmed by a black color of the solution at the end of the reaction.

However, the interaction of such released Ru species with the functional groups of the biopolymer in the  $0.5\text{Ru}-\text{Ch@SiO}_2$  catalyst, slows down their reduction to inactive  $\text{Ru}^0$  nanoparticles, so that high activity and selectivity values towards the aldehyde can be obtained (entry 7, table 1), to the point that  $0.5\text{Ru}-\text{Ch@SiO}_2$  could even operate in semi-continuous mode in a batch type reactor (Figure 3).

The herein proposed different reduction kinetics of the released ruthenium species was supported by an additional experiment performed in the presence of the  $0.5\text{Ru}-\text{Ch@SiO}_2$  catalyst. In this case a double experiment was carried out, which consisted in quenching the reaction after 1 h, and depressurizing the reactor. Then, on the one hand the solid was kept inside the reactor while in the other case it was removed. After that, the reactors were re-pressurized with 40 bar of  $\text{N}_2$  and heated to  $170^\circ\text{C}$  for 18 h. Completed the 18 h, the reaction was restarted in both cases by swapping from  $\text{N}_2$  to syngas. Interestingly, while in the first case (in the presence of the solid  $\text{Ch@SiO}_2$ ), the activity was practically recovered, in the second

case the activity was completely lost (Figure S6). In line with this result, a different solution colour was obtained at the end of reaction being yellow in the first case, while black in the last case. These results clearly confirm the stabilizing role of  $\text{Ch@SiO}_2$  avoiding a fast reduction of the released ruthenium species to  $\text{Ru}^0$ .

In a second step, the nature of the release ruthenium species of the  $0.5\text{Ru}-\text{Ch@SiO}_2$  sample has been analysed by X-ray adsorption spectroscopy (XAS).

Figure 4 shows the recorded Ru K-edge X-ray adsorption spectra of the liquid phase after hot filtration experiments using the  $0.5\text{Ru}-\text{Ch@SiO}_2$  catalyst after 1 h and 7 h reaction compared to different references (Ru metal,  $\text{Ru}_3(\text{CO})_{12}$  dissolved in NMP solution and  $\text{Ru}(\text{acac})_3$ ). The X-ray absorption near edge structure (XANES) spectra of these two liquid samples present negligible differences being very similar to that of  $\text{Ru}_3(\text{CO})_{12}$  in NMP, suggesting a similar Ru local structural and electronic environment (panel a). The inset in panel a reports the derivative of the XANES spectra around the first absorbing features. The bump around 22115 eV corresponds to the presence of  $\text{Ru}^0$  species, which is the oxidation state expected for the bulk  $\text{Ru}_3(\text{CO})_{12}$  system. The second feature around 22125 eV indicates the presence of oxidized species. Interestingly, both  $\text{Ru}_3(\text{CO})_{12}$  dissolved in NMP and the  $\text{Ru}-\text{Ch@SiO}_2$  liquid samples after hot filtration present the coexistence of  $\text{Ru}^0$  and Ru oxidized species, where the  $\text{Ru}^0$  species could correspond to remnant bulk  $\text{Ru}_3(\text{CO})_{12}$  in the solutions. Instead, the Ru oxidized species correspond to oxidized mononuclear Ru. Furthermore, the shift of the main first derivative peak toward lower energy for the  $0.5\text{Ru}-\text{Ch@SiO}_2$  liquid samples corresponds to a lower effective Ru oxidation state with respect to the  $\text{Ru}_3(\text{CO})_{12}$  in NMP system.

In panel b are reported the Fourier transforms of the  $k^2$  weighted extended x-ray absorption fine structure (EXAFS) oscillation. Four striped backgrounds represent the R regions of interest with different contributions: the Ru–O shell (around 1.5 Å), the Ru–C shell (around 1.7 Å), the Ru–N/O shell (around 2 Å), and the Ru–Ru shell (around 2.4 Å).<sup>[31–33,61, 62]</sup> Similar to the XANES, the EXAFS region of the two investigated samples is not showing significant differences. When comparing the  $0.5\text{Ru}-\text{Ch@SiO}_2$  liquid samples after hot filtration to the  $\text{Ru}_3(\text{CO})_{12}$  in NMP reference, clear spectral differences can be instead identified. In particular, the rise of spectral weight around 2 and 2.5 Å in the samples is compatible with increased presence of Ru–N/O and Ru–Ru bonds. Globally the XANES and EXAFS show the formation in the  $0.5\text{Ru}-\text{Ch@SiO}_2$  liquid samples after hot filtration of mononuclear oxidized Ru species stabilized by the interaction with N/O functional groups which may come from the amido or amino groups of the biopolymer, in coexistence with some Ru–Ru species.

The fact that EXAFS shows that N/C/O ligands could be all involved in stabilizing the ruthenium species after hot filtration, may indicate some degradation or dissolution of the chitosan polymer under the reaction conditions. Control experiments submitting the  $0.5\text{Ru}-\text{Ch@SiO}_2$  catalyst to reaction conditions but in absence of NMP (details in SI) and analysing the liquid after hot filtration, showed the presence of Ru–N, and Ru–O

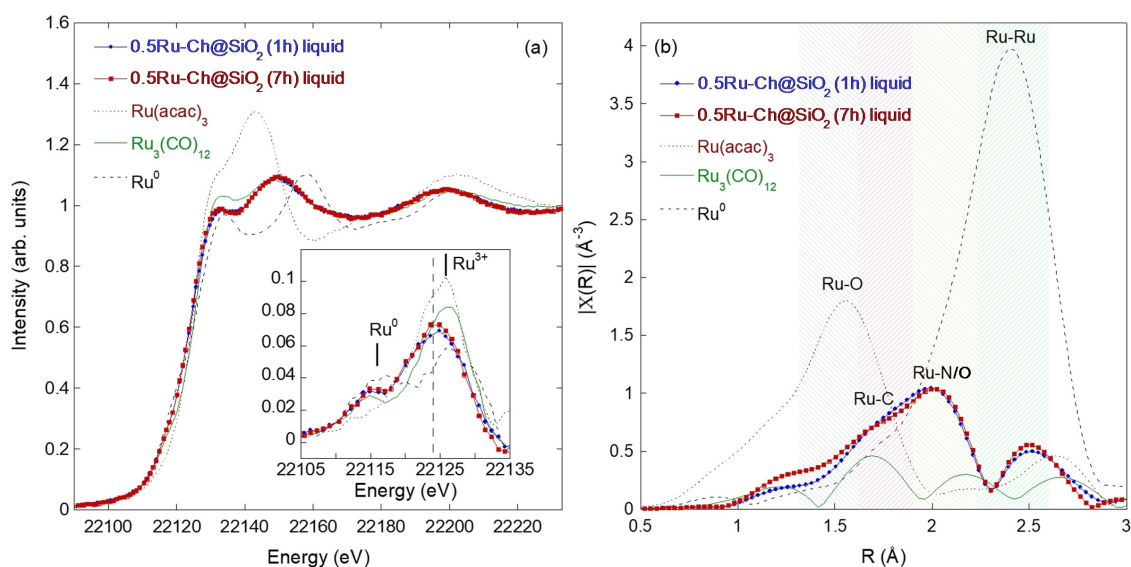


**Figure 4.** a) Ru K-edge XANES spectra collected on 0.5Ru–Ch@SiO<sub>2</sub> liquid samples after hot filtration in comparison with references (Ru metal, Ru<sub>3</sub>(CO)<sub>12</sub> in NMP solution, and Ru(acac)<sub>3</sub>). The inset depicts the first derivative of the XANES spectra in the region close to the rising edge. The energy positions corresponding to the Ru<sup>0</sup> and Ru<sup>3+</sup> phase contributions are marked. b) Fourier transforms of the *k*<sup>2</sup> weighted Ru K-edge extended x-ray absorption fine structure (EXAFS) oscillation, extracted with a sinus window in the 2.7–14.4 Å<sup>-1</sup> *k* range. Four striped backgrounds represent the R regions interested by different contributions: the Ru–O shell (around 1.5 Å), the Ru–C shell (around 1.7 Å), the Ru–N/O shell (around 2 Å), and the Ru–Ru shell (around 2.4 Å).

vibrational bands in Raman (Figure S7 and details in SI), which unambiguously has to be ascribed to the chitosan biopolymer. However, the fact that <sup>13</sup>C CP-NMR and AES analysis of the used 0.5Ru–Ch@SiO<sub>2</sub> catalyst doesn't reveal important weight losses of C, N % nor structural changes in the chitosan structure (Figure S2 and Table S1), strongly points to chitosan biopolymer being stable under reaction conditions. In this regard, it is not unrealistic that the released Ru@N/C/O species may interact with the Ch@SiO<sub>2</sub> solid through N/O binding sites of chitosan under reaction conditions explaining their stabilization under operating conditions.

### Effect of the reaction conditions on the catalytic performance

Next, the effect of the reaction conditions on the catalytic activity and stability of the ruthenium-based catalyst was investigated and results are summarized in Figure 5 and Table 2. Firstly, the effect of temperature was analyzed. From Figure 5A, it can be noted that the catalytic activity of 0.5Ru–Ch@SiO<sub>2</sub> decreases when lowering temperature from a TOF of 1603 h<sup>-1</sup> to 387 h<sup>-1</sup> at 190 °C and 150 °C respectively. A closer look to the product composition (Figure 5D) shows that a decrease in reaction temperature increases the regioselectivity affording the highest linear to branched ratio 95:5. On the

**Table 2.** [a] Reaction conditions: 3.2 mmol 1-hexene, 2 mL NMP, 0.7 mmol iso-octane (internal standard), 0.022% mmol Ru (2.56 μmol Ru/g 1-hexene) as Ru<sub>3</sub>(CO)<sub>12</sub>, 14 mg of catalyst, 40 bar CO:H<sub>2</sub> (1:1), 170 °C, 750 r.p.m, 7 h; [b] Linear to branched product ratio; [c] mmol of aldehyde/total mmol of Ru after 7 h of reaction; [d] rate of formation of aldehyde/total mmol of Ru; [e] Ru<sub>3</sub>(CO)<sub>12</sub> was not added; instead only 14 mg of 0.5Ru–Ch@SiO<sub>2</sub> were used; [f] Toluene (2 mL) was used instead of NMP as solvent. Table 2

Effect of different reaction conditions on the aldehyde selectivity and catalytic performance of 0.5Ru–Ch@SiO<sub>2</sub> during the hydroformylation of 1-hexene.<sup>[a]</sup>

Entry	Reaction Conditions		CO:H <sub>2</sub> Mol Ratio (-)	Selectivity [%] 2 (n:iso) <sup>[b]</sup>	TON <sup>[c]</sup> (-)	TOF <sup>[d]</sup> [h <sup>-1</sup> ]
	T [°C]	P [bar]				
1	150	40	1:1	63 (95:5)	1824	358
2	170			66 (92:8)	2749	1086
3	190			48 (89:11)	2967	1603
4	170	20	1:1	53 (92:8)	1943	789
5		30		61 (91:9)	2398	841
6		40		66 (92:8)	2749	1086
7	170	40	1:3	59 (92:8)	2602	878
8			1:1	66 (92:8)	2749	1086
9			3:1	85 (91:9)	1845	629

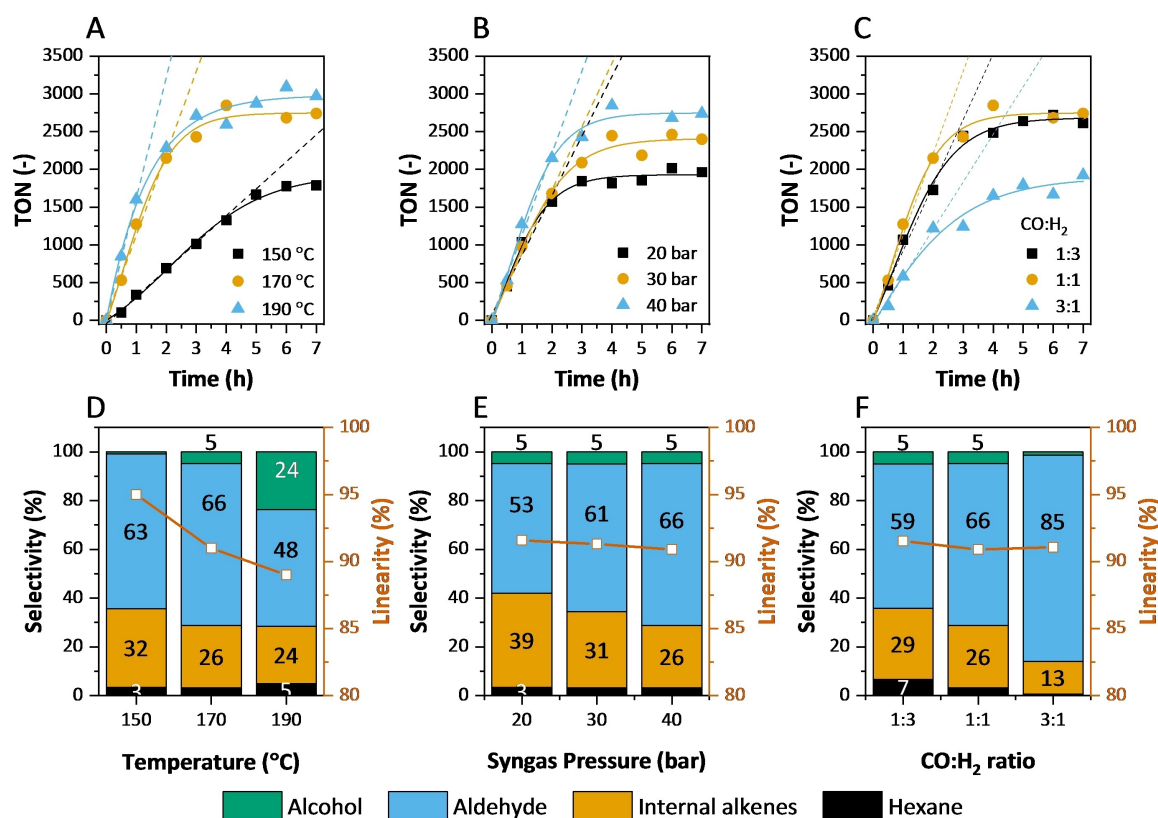


**Figure 5.** Summary of the effect of the temperature, syngas pressure and gas composition on activity (A, B and C) and product composition (D, E and F) respectively during the 1-hydroformylation of 1-hexene catalyzed by 0.5Ru–Ch@SiO<sub>2</sub>.

contrary, an increase of reaction temperature leads to the hydrogenation of the formed aldehydes to the respective alcohols.

Then, the influence of the syngas partial pressure at 170 °C was also studied (Figures 5B and 5E). In this case, in order to keep the total reactor pressure constant when varying the syngas partial pressure in the series of experiments, the reactor was always kept at a total pressure of 40 bar by using N<sub>2</sub> as the pressure compensating gas. In this case, an increase in syngas pressure led to a slight increase in the catalytic behavior of the Ru based catalyst from 789 h<sup>-1</sup> to 1086 h<sup>-1</sup> at 20 bar and 40 bar respectively. The fact that the Ru species are still able to carry out the hydroformylation of 1-hexene at P<sub>CO</sub> as low as 10 bar is a proof of the stabilizing role of the Ch@SiO<sub>2</sub> support by preventing the otherwise reduction of Ru<sub>3</sub>(CO)<sub>12</sub> to inactive Ru<sup>0</sup> NPs when operating under homogeneous conditions.

Lastly, the impact of the composition of the gas mixture at 170 °C was also examined. From Figure 5C it can be distinguished how an increase in the H<sub>2</sub> partial pressure has a slight negative effect on the hydroformylation activity while the hydrogenating ability of the catalysts is slightly enhanced. Remarkably, when the P<sub>CO</sub> is increased the selectivity towards the hydroformylation increases from 66% to 85% although at the expense of decreasing the TOF to 629 h<sup>-1</sup>.

According to these results, the final product of the reaction can be easily tuned by modifying the operating condition of

the reactor, maintaining similar chemo-selectivity across a wide range of temperatures, pressures, and gas compositions.

## Conclusions

This study reveals an interesting and easy strategy to prepare a cheap, non-toxic hydroformylating catalyst by using a natural biopolymer, i.e. chitosan, supported on an inorganic material, SiO<sub>2</sub>, which behaves as a soft and recoverable ligand of a homogeneous Ru<sub>3</sub>(CO)<sub>12</sub> counterpart. Definitely, it appears that the reaction is neither completely homogeneous, nor completely heterogeneous so that it could be taking place at the liquid/solid interface in a kind of biphasic system.

IR and XAS studies reveals that the Ru<sub>3</sub>(CO)<sub>12</sub> precursor transforms into a mononuclear Ru<sup>n+</sup> (n=2,3) di or tricarbonyl complex, when supported on the Ch@SiO<sub>2</sub> catalyst. Under reaction conditions, ruthenium is released to the reaction media resulting in the formation of mononuclear oxidized Ru species stabilized by the interaction with the amido or amino groups coming from the biopolymer, as revealed from the EXAFS and Raman analysis, in coexistence with some Ru–Ru species. The weak binding interaction between the released Ru species and the Ch@SiO<sub>2</sub> composite results in an enhanced stability and chemo and regioselectivity compared to the unmodified homogeneous Ru<sub>3</sub>(CO)<sub>12</sub> counterpart and that of a physical

mixture of each of the incorporated components separately. In particular, TOF of  $1087\text{ h}^{-1}$  and regioselectivities up to  $n:\text{iso} = 92:8$  are obtained. These values are superior to those reported for the homogeneous unmodified  $\text{Ru}_3(\text{CO})_{12}$  component ( $180\text{ h}^{-1}$  and  $83:17$   $n:\text{iso}$  ratio). Moreover, unlike phosphines and other classical hydroformylation ligands, the  $\text{Ch@SiO}_2$  hybrid can be easily separated and recovered from the reaction medium behaving as a soft and green ligand.

Moreover, the catalyst is stable under reaction conditions and can be operated under a semi-continuous mode for at least 14 h without deactivation. In addition, the reaction can be directed towards obtaining one final product or another by simply modifying the reaction conditions. That is, we can move from linear aldehydes (high  $P_{\text{CO}}$  and lower temperature) to linear alcohols (low  $P_{\text{CO}}$  and higher temperature) while maintaining similar chemoselectivity across a wide range of temperatures, pressures and gas compositions.

In summary, the use of the  $\text{Ru}-\text{Ch@SiO}_2$  nanocomposite represents a starting point in the search for a green and definitive heterogeneous catalyst away from the use of phosphines and expensive rhodium. Certainly, this approach will help design and define future catalytic systems for carbonylation reactions.

## Methods/Experimental Section

### Chemicals and reagents

The reagents used were supplied by Sigma-Aldrich and were used without any further purification. Silicon oxide ( $\text{SiO}_2$ ) was supplied by Evonik. Aerosil 200 with a surface area of  $275\text{ m}^2/\text{g}$  was used.  $\text{Ru}_3(\text{CO})_{12}$  was supplied by ABCR. The reaction gas mixture  $\text{CO}:\text{H}_2$  (1:1) was supplied by Abello-Linde.

### Synthesis of the chitosan-silica hybrid $\text{Ch@SiO}_2$

The chitosan-silica hybrid  $\text{Ch@SiO}_2$  was prepared following a previously described methodology with minor modifications.<sup>[46,49]</sup> First, 0.2 g of low molecular weight chitosan with a deacetylation degree of 77% were dissolved in 200 mL of milliQ water and 3 mL of acetic acid were added, giving rise to a final concentration of 1.5% (v/v) of the acid. The mixture was stirred at room temperature for 24 h until the complete dissolution of the biopolymer. In a second step, 1 g of silica Aerosil 200, was incorporated under vigorous stirring. Stirring was maintained for 0.5 h until a homogeneous suspension was obtained. Then sodium hydroxide, NaOH, 1 M was added until  $\text{pH} = 13$ . At this pH the precipitation of chitosan on silica took place, giving rise to the hybrid material  $\text{Ch@SiO}_2$ , which was filtered, washed with 2 L of distilled water up to a neutral pH. Then, The solid was dried in an oven at  $100^\circ\text{C}$  for 12 h.

### Synthesis of 0.5Ru-Ch@SiO<sub>2</sub> catalyst

10.6 mg of  $\text{Ru}_3(\text{CO})_{12}$  was dissolved in n-pentane and then 1.0 g of  $\text{Ch@SiO}_2$  was incorporated.<sup>[49]</sup> The suspensions were kept for 12 h under stirring at reflux temperature. The solvent was evaporated under reduced pressure. The catalysts were used directly without further treatment.

### Hydroformylation of alkenes

The hydroformylation reaction was carried out with 1-hexene as model substrate. The reaction was carried out in a stainless steel autoclave-type reactor equipped with a PEEK (poly-ether ether ketone) jacket. The autoclave was modified to allow sampling during the reaction at high pressure. In general, 14 mg of catalyst, 2 mL of N-methyl pyrrolidone (NMP),<sup>[63]</sup> 80 mg of cyclohexane (0.95 mmol, as internal standard) and 270 mg of 1-hexene (3.2 mmol). The reactor was closed, purged 3 times with 10 bar with synthesis gas ( $\text{CO}:\text{H}_2$  ratio 1:1) before being pressurized to the final pressure of 40 bar and finally heated to  $175^\circ\text{C}$ . In the case of homogeneous reactions, the necessary amount of the precatalyst  $\text{Ru}_3(\text{CO})_{12}$  was dissolved in NMP and then added to the reactor as described above.

It is necessary to highlight that NMP has a wide range of uses due to the following excellent characteristics: a) highly polar and miscible with most organic solvents (alcohols, ethers, ketones, aromatic hydrocarbons, chlorinated hydrocarbons, etc.). Both organic and inorganic substances are highly soluble in it; b) miscible with water in all proportions; c) high flash point compared to similar solvents; d) high boiling point, low freezing point, and easy handling; e) chemically and thermally stable, and not corrosive.

### Hot Filtration Procedure

The reaction was cooled to  $50^\circ\text{C}$  to prevent evaporation of 1-hexene, iso-hexenes, hexane, and cyclohexane given that the hot mixture was withdrawn at high pressure from inside the reactor. The reaction was then filtered through a preheated filter system. The liquid was added to a new reactor, previously washed with acid, and the reaction was monitored by GC following the procedure described above. The solid was filtered and washed with dichloromethane, dried in an oven at  $60^\circ\text{C}$  for 12 h and reused in reaction following the reaction procedure previously described.

### Semicontinuous operation

To simulate continuous operation, 270 mg (3.2 mmol) of 1-hexene were added at the end of reaction using a Hamilton-type syringe through the pressurized sampling cannula and the reaction was continued without repressurization of the reactor. The reaction was monitored by GC.

### Spectroscopic characterization of the catalysts

#### X-ray adsorption analysis

Ru K-edge x-ray absorption spectra were collected at the CL $\text{ESS}$  beamline of the ALBA synchrotron.<sup>[64]</sup> The synchrotron radiation was monochromatized by means of a double crystal Si(311) monochromator, with higher harmonics rejected by choosing the proper angles and coatings for the collimating and focusing mirrors. The absorption data were acquired in fluorescence mode for the liquid samples and in transmission mode for the solid references. For the latter the powdered samples were mixed uniformly in a boron nitride matrix and pressed into pellets to ensure an absorption jump close to 1. Several scans were measured to ensure reproducibility and a good signal to noise ratio. The data were treated with the Demeter package and the energy was calibrated to the first inflection point of the Ru metal spectrum taken as  $22117\text{ eV}$ .<sup>[65]</sup>

### IR and Raman analysis

Infrared (IR) spectra were recorded with a Nicolet (Nexus) 8700 FTIR spectrometer using a DTGS detector and acquiring at  $4\text{ cm}^{-1}$  resolution. For liquid samples a drop of the solution was placed on a Ge disc and analysed after air evaporation. For solid samples, 10 mg of the solid was pressed into a disc and analysed by IR.

Raman spectra were collected with an "in via" Renishaw spectrometer equipped with an Olympus microscope. The samples were analysed using an 785 nm excitation laser with a laser power of 2.5 mW. For analysis a drop of the liquid solution was placed on a copper plate and analysed after air evaporation. Spectra at different points are adquired in order to analyse sample homogeneity.

### Acknowledgements

This research was funded by Ministerio de Ciencia, Innovación y Universidades, Grants number RTI2018-099668-B-C21 and PGC2018-101247-B-100, and Generalitat Valenciana (GVA), AICO/2020/205. F.J.E.B acknowledges the Polytechnical University of Valencia for the economic support through the grant of an FPI scholarship associated with the PAID programme "Programa de Ayudas de Investigación y Desarrollo". XAS experiments were performed at the BL22-CLÆSS beamline at the ALBA Synchrotron with the collaboration of ALBA staff as part of projects 2019093692 and 2020024106.

### Conflict of Interest

The authors declare no conflict of interest.

### Data Availability Statement

The data that support the findings of this study are available in the supplementary material of this article.

**Keywords:** chitosan · hydroformylation · regioselective · ruthenium ·  $\text{Ru}_3(\text{CO})_{12}$  · soft ligand

- [1] B. Cornils, W. A. Herrmann, M. Rasch, *Angew. Chem. Int. Ed. Engl.* **1994**, *33*, 2144–2163.
- [2] A. Börner, R. Franke, *Hydroformylation: Fundamentals, Processes and Application in Organic Synthesis*, VCH: Weinheim, Germany, **2016**.
- [3] G. T. Whiteker, C. J. Copley, *Top. Organomet. Chem.* **2012**, *42*, 35–46.
- [4] E. V. Gusevskaya, J. Jimenez-Pinto, A. Börner, *ChemCatChem* **2014**, *6*, 382–411.
- [5] L. H. Slaugh, R. D. Mullineaux, *J. Organomet. Chem.* **1968**, *13*, 469–477.
- [6] R. L. Pruett, J. A. Smith, *J. Org. Chem.* **1969**, *34*, 327–330.
- [7] W. Keim, *Angew. Chem. Int. Ed.* **2013**, *52*, 12492–12496.
- [8] J. C. Mol, *J. Mol. Catal. A* **2004**, *213*(1), 39–45.
- [9] D. Evans, J. A. Osborn, G. Wilkinson, *J. Chem. Soc. A* **1968**, 3133–3142.
- [10] R. Dühren, P. Kucmierczyk, C. Schneider, R. Franke, M. Beller, *Catal. Sci. Technol.* **2021**, *11*, 5777–5780.
- [11] R. Dühren, P. Kucmierczyk, R. Jackstell, R. Franke, M. Beller, *Catal. Sci. Technol.* **2021**, *11*, 2026–2030.
- [12] F. M. S. Rodrigues, P. K. Kucmierczyk, M. Pineiro, R. Jackstell, R. Franke, M. M. Pereira, M. Beller, *ChemSusChem* **2018**, *11*, 2310–2314.
- [13] C. Rodrigues, F. G. Delolo, J. Norinder, A. Börner, A. L. Bogado, A. A. Batista, *J. Mol. Catal. A* **2017**, *426B*, 586–592.
- [14] M. Vilches-Herrera, L. Domke, A. Börner, *ACS Catal.* **2014**, *4*(6), 1706–1724.
- [15] Y. Yuki, K. Takahashi, Y. Tanaka, K. Nozaki, *J. Am. Chem. Soc.* **2013**, *135*, 17393–17400.
- [16] R. Franke, D. Selent, A. Börner, *Chem. Rev.* **2012**, *112*, 5675–5732.
- [17] K. Takahashi, M. Yamashita, T. Ichihara, K. Nakano, K. Nozaki, *Angew. Chem. Int. Ed.* **2010**, *49*, 4488–4490.
- [18] L. Diab, T. Smejkal, J. Geier, B. Breit, *Angew. Chem. Int. Ed.* **2009**, *48*, 8022–8026.
- [19] P. C. J. Kamer, P. W. N. M. van Leeuwen, *Phosphorus(III) Ligands in Homogeneous Catalysis*, Eds. Wiley: Chichester, UK, **2012**.
- [20] S. Dastgir, K. S. Coleman, M. L. H. Green, *Dalton Trans.* **2011**, *40*, 661–672.
- [21] L. Alvila, T. A. Pakkaken, O. Krause, *J. Mol. Catal.* **1993**, *84*, 145–156.
- [22] T. Mitsudo, N. Suzuki, T. Kondo, Y. Watanabe, *J. Mol. Catal. A* **1996**, *109*, 219–225.
- [23] T. Mitsudo, N. Suzuki, T. Kobayashi, T. Kondo, *J. Mol. Catal. A* **1999**, *137*, 253–262.
- [24] F. P. Pruchnik, S. A. Duraj, *Organometallic Chemistry of the Transition Elements*, Springer US, **1990**.
- [25] W. Ren, W. Chang, J. Dai, Y. Shi, J. Li, Y. Shi, *ACS Catal.* **2016**, *138*(45), 14864–14867.
- [26] Y. Zhang, S. Torker, M. Sigrist, N. Bregović, P. Dydio, *J. Am. Chem. Soc.* **2020**, *142*(42), 18251–18265.
- [27] L. Liu, H. Gao, S.-Q. Yang, X. C. Chen, Y. Lu, Y. Liu, F. Xia, *J. Catal.* **2020**, *385*, 183–193.
- [28] C. Breschi, L. Piparo, P. Pertici, A. M. Caporusso, G. Vitulli, *J. Organomet. Chem.* **2000**, *607*, 57–63.
- [29] L. Kollár, G. Keglevich, *Chem. Rev.* **2010**, *110*, 4257–4302.
- [30] P. Pongrácz, L. Kollár, A. Kerényi, V. Kovács, V. Ujj, G. Keglevich, *J. Organomet. Chem.* **2011**, *696*, 2234–2237.
- [31] J. Pospech, I. Fleischer, R. Franke, S. Buchholz, M. Beller, *Angew. Chem. Int. Ed.* **2013**, *52*, 2852–2872.
- [32] F.-J. Escobar-Bedia, M. Lopez-Haro, J. J. Calvino, V. M. Diaconescu, L. Simonelli, V. Perez-Dieste, M. J. Sabater, P. Concepción, A. Corma, *ACS Catal.* **2022**, *12*, 4182–4193.
- [33] S. Pandey, K. Vipin Raj, D. R. Shinde, K. Vanka, V. Kashyap, S. Kurungot, C. P. Vinod, S. H. Chikkali, *J. Am. Chem. Soc.* **2018**, *140*(12), 4430–4439.
- [34] R. Kumar, S. H. Chikkali, *J. Organomet. Chem.* **2022**, *960*, 122231.
- [35] G. Süß-Fink, *J. Organomet. Chem.* **1980**, *193*(1), C20–C22.
- [36] R. A. Sanchez-Delgado, J. S. Bradley, G. Wilkinson, *J. C. S. Dalton* **1980**, 399–404.
- [37] A. Fusi, E. Cesarotti, R. Ugo, *J. Mol. Catal.* **1981**, *10*(2), 213–221.
- [38] A. Kämper, P. Kucmierczyk, T. Seidensticker, A. J. Vorholt, R. Franke, A. Behr, *Catal. Sci. Technol.* **2016**, *6*, 8072–8079.
- [39] L. Wu, I. Fleischer, R. Jackstell, I. Profir, R. Franke, M. Beller, *J. Am. Chem. Soc.* **2013**, *135*, 14306–14312.
- [40] J. Liu, C. Kubis, R. Franke, R. Jackstell, M. Beller, *ACS Catal.* **2016**, *6*(2), 907–912.
- [41] L. Le Goanvic, J. L. Couturier, J. L. Dubois, J. F. Carpentier, *J. Mol. Catal. A* **2016**, *417*, 116–121.
- [42] P. Wang, D.-L. Wang, H. Liu, X.-L. Zhao, Y. Lu, Y. Liu, *Organometallics* **2017**, *36*(13), 2404–2413.
- [43] J. October, S. F. Mapolie, *J. Organomet. Chem.* **2017**, *840*, 1–10.
- [44] a) I. Fleischer, L. Wu, I. Profir, R. Jackstell, R. Franke, M. Beller, *Chem. A Eur. J.* **2013**, *19*, 10589–10594; b) G. R. F. Orton, D. S. Pilgrim, N. R. Champness, *Chem. Soc. Rev.* **2021**, *50*, 4411–4431.
- [45] S. Sartipi, M. J. Valero Romero, E. Rozhko, Z. Que, H. A. Stil, J. de With, F. Kapteijn, J. Gascón, *ChemCatChem* **2015**, *7*, 3243–3247.
- [46] M. Y. Yin, G. L. Yuan, Y. Q. Wu, M. Y. Huang, Y. Y. Jiang, *Proceedings of the Journal of Molecular Catalysis A: Chemical*; Elsevier, **1999**, *147*, 93–98.
- [47] M. J. Sabater, T. Ródenas, A. Heredia, *Biopolymers from Plants*. In *Handbook of Biopolymer-Based Materials: From Blends and Composites to Gels and Complex Networks*; Thomas, S.; Durand, D.; Chassenieux, C.; Jyotishkumar, P.; Ed.; Wiley Online Books; John Wiley & Sons, Inc, **2013**, 37–86.
- [48] V. Wankhade, *Animal-derived biopolymers in food and biomedical technology*. In *Biopolymer-Based Formulations*, Elsevier. Inc., **2020**, 139–152.
- [49] A. Corma, P. Concepción, I. Domínguez, V. Fornés, M. J. Sabater, *J. Catal.* **2007**, *259*(1), 39–57.
- [50] B. Zhang, D. Peña Fuentes, A. Börner, *ChemTexts* **2022**, *8*, <https://doi.org/10.1007/s40828-021-00154-x>.

- [51] K. Tominaga, Y. Sasaki, *Catal. Commun.* **2000**, *1*, 1–3.
- [52] S. Fujita, S. Okamura, Y. Akiyama, M. Arai, *Int. J. Mol. Sci.* **2007**, *8*, 749–759.
- [53] X. Ren, Z. Zheng, L. Zhang, Z. Wang, C. Xia, K. Ding, *Angew. Chem. Int. Ed.* **2017**, *56*, 310–313.
- [54] <https://pubchem.ncbi.nlm.nih.gov/compound/Ruthenium-dodecacarbonyltri-triangulo#section=FTIR-Spectra>.
- [55] K. Asakura, K.-K. Bando, Y. Iwasawa, *J. Chem. Soc. Faraday Trans.* **1990**, *86*, 2645–2655.
- [56] A. Zecchina, E. Guglielminotti, A. Bossi, M. Camia, *J. Catal.* **1982**, *74*(2), 225–239.
- [57] J. Evans, G. S. McNulty, *J. Chem. Soc. Dalton Trans.* **1984**, 1123–1131.
- [58] O. A. M. Ali, L.-H. Abdel-Rahman, R. M. Ramadan, *J. Coord. Chem.* **2007**, *60*, 2335–2342.
- [59] K. I. Hadjiivanov, G. N. Vayssilov, *Adv. Catal.* **2002**, *47*, 307–511.
- [60] M. Y. Mihaylov, O. V. Lagunov, E. Ivanova, K. I. Hadjiivanov, *J. Phys. Chem. C* **2011**, *115*(18), 13860–13867.
- [61] C. Zhang, J. Sha, H. Fei, M. Liu, S. Yazdi, J. Zhang, Q. Zhong, X. Zou, N. Zhao, H. Yu, Z. Jiang, E. Ringe, B. I. Yakobson, J. Dong, D. Chen, J. M. Tour, *ACS Nano* **2017**, *11*, 6930–6941.
- [62] A. A. Adeniyi, P. A. Ajibade, *J. Chem.* **2016**, 1–15, 10.1155/2016/3672062.
- [63] NMP has a wide range of uses due to the following excellent characteristics: a) highly polar and miscible with most organic solvents (alcohols, ethers, ketones, aromatic hydrocarbons, chlorinated hydrocarbons, etc.). Both organic and inorganic substances are highly soluble in it; b) miscible with water in all proportions; c) high flash point compared to similar solvents; d) high boiling point, low freezing point and easy handling; e) chemically and thermally stable, and not corrosive: N. S. Basma, T. F. Headen, M. S. P. Shaffer, N. T. Skipper, C. A. Howard, *J. Phys. Chem. C* **2018**, *122*(38), 8963–8971.
- [64] L. Simonelli, C. Marini, W. Olszewski, M. Avila Perez, N. Ramanan, G. Guilera, V. Cuartero, K. Klementiev, *Cogent Phys* **2016**, *3*, 1231987.
- [65] B. Ravel, M. Newville, *J. Synchrotron Radiat.* **2005**, *12*, 537–541.

---

Manuscript received: July 15, 2022

Revised manuscript received: September 29, 2022

Accepted manuscript online: October 19, 2022

Version of record online: November 17, 2022